

Supporting Information for

Enriching the Branchness of Au@PdAu Core-Shell Nanocrystals Using a Syringe Pump: Kinetics Control Meets Lattice Mismatch

Gongguo Zhang,^a Yanyun Ma,^{*b} Xiaowei Fu,^a Wenjun Zhao,^a Feng Liu,^c Maochang Liu,^c and Yiqun Zheng^{*a}

^a Department of Chemistry and Chemical Engineering, Jining University, Qufu, Shandong 273155, P. R. China.

^b Institute of Functional Nano & Soft Materials (FUNSOM), Jiangsu Key Laboratory for Carbon-Based Functional Materials & Devices, Soochow University, Suzhou, Jiangsu 215123, P. R. China.

^c International Research Center for Renewable Energy, National Key Laboratory of Multiphase Flow in Power Engineering, Xi'an Jiaotong University, Xi'an, Shanxi 710049, China

*Corresponding Author:

Prof. Dr. Y. Zheng, E-mail: whzyq@163.com; Prof. Dr. Y. Ma, E-mail: mayanyun@suda.edu.cn

Number of Page: 20; Number of Figure: 15; Number of Table: 2.

Table of Content

Experimental Details: Materials; Standard Synthetic Procedure; Instruments; Electrochemical Measurement.

Figure S1. SEM image of the products obtained via the standard procedure, except that the bimetallic precursor solution was dropwise added at the injection rate of 1 mL/h.

Figure S2. Histogram showing the size distribution of Au@PdAu core-shell nanocrystals in the form of concave cube.

Figure S3. XRD pattern of Au@PdAu core-shell nanocrystals in the form of concave cube.

Figure S4. EDS spectrum of Au@PdAu core-shell nanocrystals in the form of concave cube.

Figure S5. Histogram showing the size distribution of Au@PdAu core-shell nanocrystals in the form of dendrites.

Figure S6. XRD pattern of Au@PdAu core-shell nanocrystals in the form of dendrites.

Figure S7. EDS spectrum of Au@PdAu core-shell nanocrystals in the form of dendrites.

Figure S8. XPS spectra of Au@PdAu nano-dendrites.

Figure S9. TEM images of Au@PdAu products with tunable sizes.

Figure S10. Histogram showing the size distribution of Au@PdAu core-shell nanocrystals in the form of segmented branches.

Figure S11. XRD pattern of Au@PdAu core-shell nanocrystals in the form of segmented branches.

Figure S12. EDS spectrum of Au@PdAu core-shell nanocrystals in the form of segmented branches.

Figure S13. UV-vis extinction spectra of Au@PdAu nanocrystals with different morphologies.

Figure S14. UV-vis extinction spectra of products as displayed in Figure 5.

Figure S15. Electrochemical performance of Pd/C catalysts for EOR.

Table S1. Synthetic parameters of products as displayed in current work.

Table S2. Summary of EOR catalytic performance for electrocatalysts in the present study.

References.

Experimental Details

Materials

Gold(III) chloride trihydrate ($\text{HAuCl}_4 \cdot 3\text{H}_2\text{O}$, 99.9%), sodium tetrachloropalladate(II) (Na_2PdCl_4 , 98%), ascorbic acid (AA, 99.0%), cetyltrimethylammonium chloride (CTAC, 97%), and cetyltrimethylammonium bromide (CTAB, 99%) were all obtained from Aladdin Chemical (Shanghai, China) and used as received. Carbon black (XC-72) was obtained from Cabot Corp. Ethanol ($\geq 95\%$), sodium borohydride (NaBH_4 , AR) and potassium hydroxide (KOH , $\geq 85.0\%$) were obtained from Sinopharm (Shanghai, China) and used as received. Nafion solution (5% wt%) was obtained from Cool Chemistry (Beijing, China) and used as received. In all experiments, we used deionized water with a resistivity of $18.2 \text{ M}\Omega \cdot \text{cm}$, which was prepared using an ultrapure water system (Ulupure, China).

Standard Procedure for the Synthesis of Dendritic Au@PdAu Core-Shell Nanocrystals

Spherical Au seeds with 10 nm in diameter were generated *via* the method documented in the previous study.^{1, 2} Then, aqueous solutions of CTAC (200 mM, 2 mL), as-prepared 10-nm Au seed stock solution (20 μL), and AA (100 mM, 0.2 mL) were sequentially mixed in a 20 mL glass vial, followed by the dropwise addition of 2 mL of aqueous solution containing HAuCl_4 and Na_2PdCl_4 with the concentration of 0.5 mM using a syringe pump at the injection rate of 2 mL/h. The Au/Pd mixed solution was prepared by mixing 0.5 mL of aqueous HAuCl_4 solution (20 mM), 0.5 mL of aqueous Na_2PdCl_4 solution (20 mM) and 19 mL of water in a glass vial and aging overnight. The reaction was conducted in a water bath set at 60 °C and allowed to proceed for 1 h after the addition was completed. The products were collected by centrifugation (16000 rpm, 5 min) and washed with water once prior to further characterization and use. For control experiments, the procedure was the same except for changing one reaction parameters while keeping others unchanged. See Table S1 for details.

Instrumentation

Transmission electron microscopy (TEM) were captured using a JEM-2100Plus (JEOL, Japan) operated at 200 kV accelerating voltage. High-resolution TEM (HRTEM), high angle

annular dark field-scanning transmission electron microscopy (HAADF-STEM) and EDX-STEM mapping images were obtained using a TALOS F200X (FEI, USA) microscope operated at 200 kV accelerating voltage. Scanning electron microscopy (SEM) images were obtained using a Zeiss Ultra60 microscope operated at 12 kV. The crystalline structures were analyzed with a MiniFlex600 X-ray diffractometer (XRD, Rigaku). X-ray photoelectron spectroscopy (XPS) measurements were performed using a Thermo Fisher Scientific KALPHA XPS with monochromatic Al K_α radiation ($h\nu=1486.6$ eV). All extinction spectra were recorded using a T9 dual-beam UV-vis-NIR spectrometer (PERSEE, China). Inductively coupled plasma analysis was conducted on an ICAP-5000 inductively coupled plasma optical emission spectrometer (Focused Photonics Instrument, China).

Electrochemical measurements

Electrochemical experiments of ethanol oxidation reaction (EOR) were carried out in a standard three-electrode system controlled by a CHI-760E potentiostat (CHI Instruments, China). A glassy-carbon electrode (3 mm in diameter), a saturated calomel electrode (SCE), and a graphite rod were used as the working-, reference-, and counter-electrode, respectively. 1 mg (in terms of Pd mass) of as-prepared Au@PdAu nanocrystals and 2 mg of carbon black were dispersed in 1 mL of water and vigorously sonicated for 30 min to form a uniform ink. Subsequently, 3 μ L of the catalyst ink was drop-cast onto the glassy carbon electrode and dried naturally, followed by dropping 3 μ L of Nafion solution and dried naturally.

Prior to EOR measurements, electro-catalysts were first activated in nitrogen-saturated aqueous KOH solution (1 M) by CV cycling between -1.0 and 0.6 V *versus* SCE at a scan rate of 200 mV s⁻¹ until the reproducible curves were obtained. CV curves in aqueous KOH solution (1 M) with or without ethanol (1 M) were then collected at 20 mV s⁻¹. The chronoamperometric (CA) curves were recorded under a constant potential of -0.2 V *versus* SCE. ECSA was estimated from the CV curve in aqueous KOH solution (1 M) using the following equation:

$$ECSA = \frac{Q_{PdO}}{0.405 \text{ mC} \cdot \text{cm}^{-2} \times m_{Pd}}$$

where Q_{PdO} was the charge by integrating the reduction peak area of PdO to Pd, m_{Pd} was the mass of Pd on the working electrode as determined by ICP-OES, respectively, $0.405 \text{ mC}\cdot\text{cm}^{-2}$ was the charge required for the reduction of PdO monolayer.³

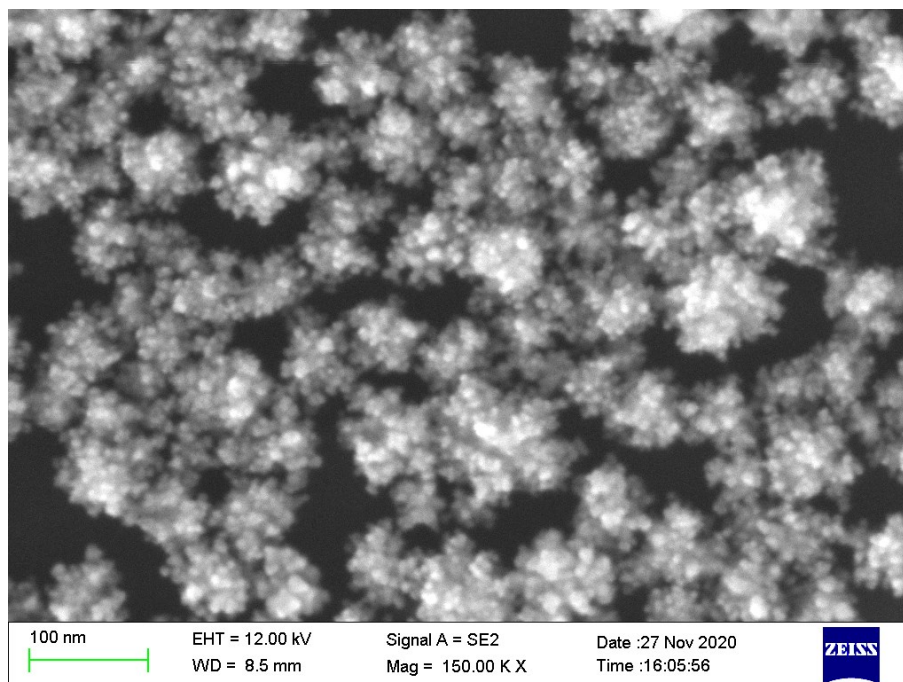


Figure S1. SEM image of the products obtained via the standard procedure, except that the bimetallic precursor solution was dropwise added using a syringe pump, at the injection rate of 1 mL/h.

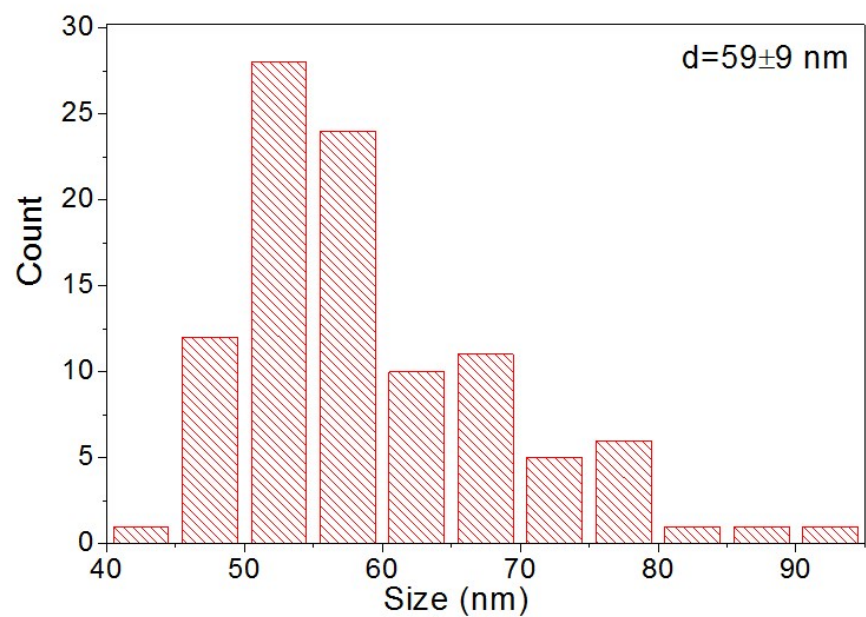


Figure S2. Histogram showing the size distribution of Au@PdAu core-shell nanocrystals in the form of concave cube.

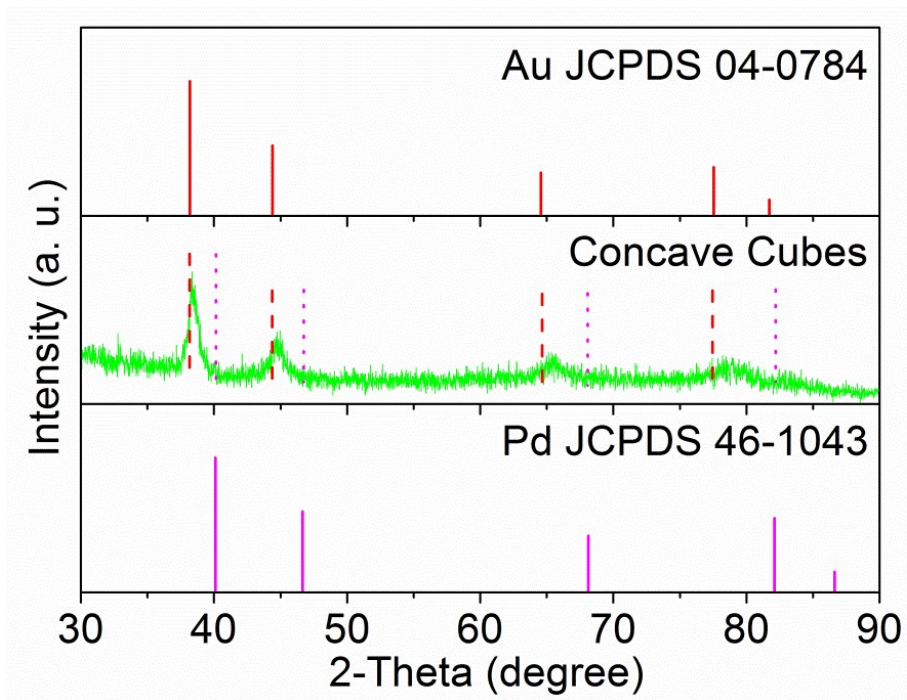


Figure S3. XRD pattern of Au@PdAu core-shell nanocrystals in the form of concave cube.

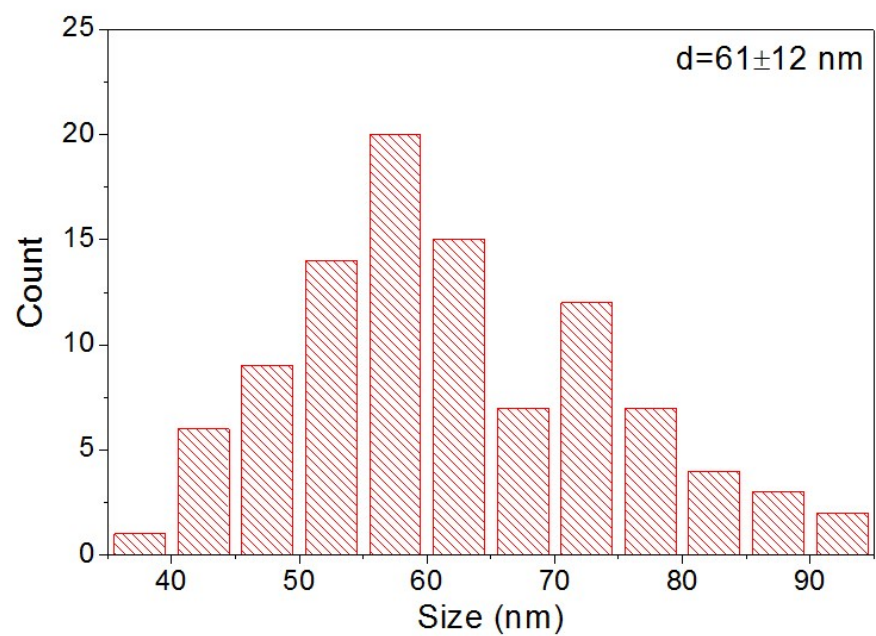


Figure S5. Histogram showing the size distribution of Au@PdAu core-shell nanocrystals in the form of dendrites.

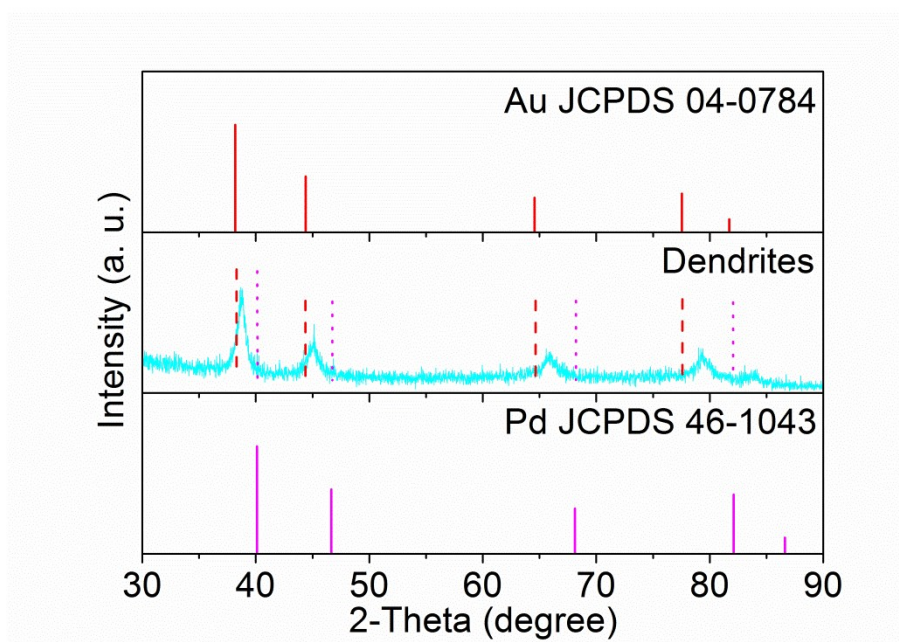


Figure S6. XRD pattern of Au@PdAu core-shell nanocrystals in the form of dendrites.

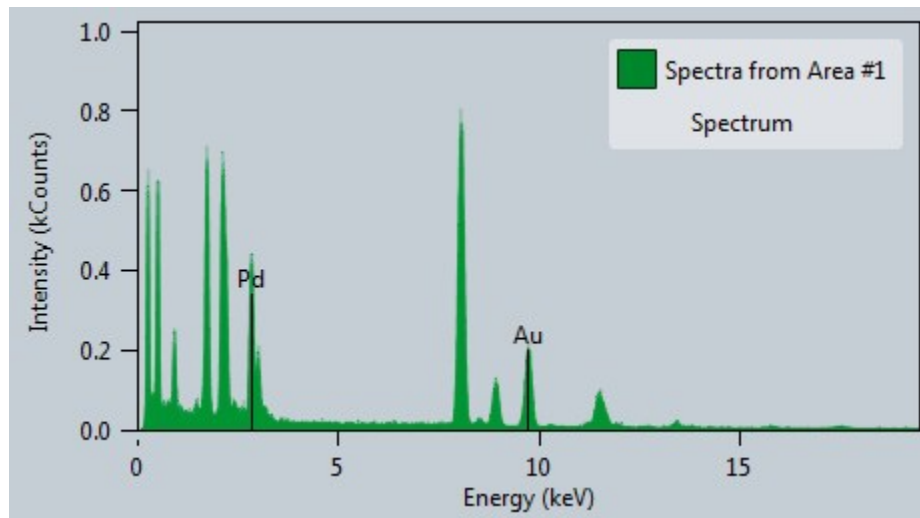


Figure S7. EDS spectrum of Au@PdAu core-shell nanocrystals in the form of dendrites.

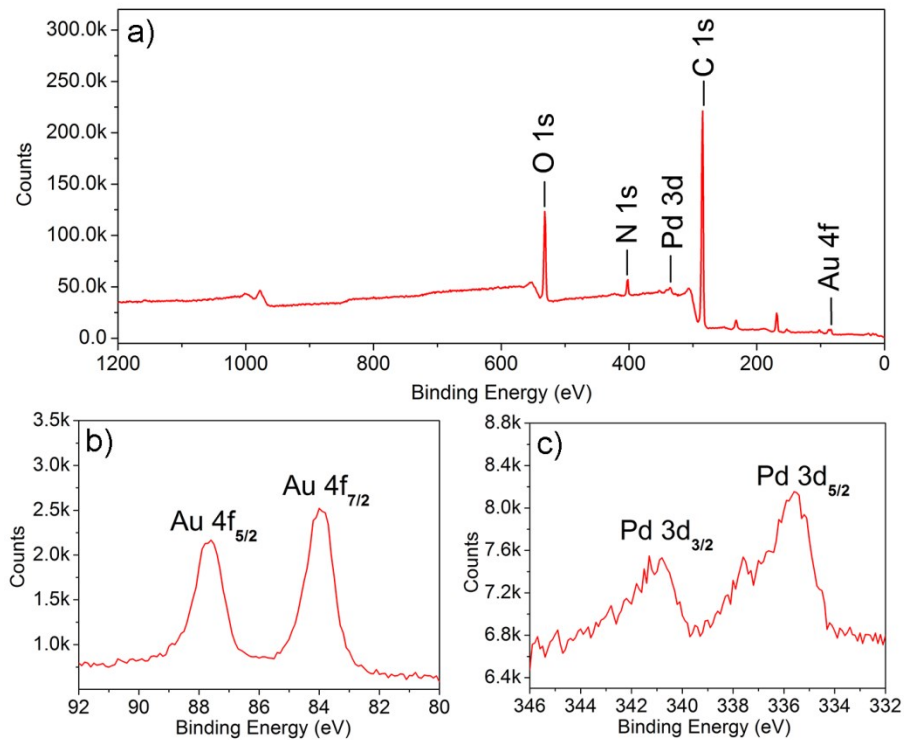


Figure S8. XPS spectra of Au@PdAu nano-dendrites: a) survey scan; b) Au 4f; c) Pd 3d.

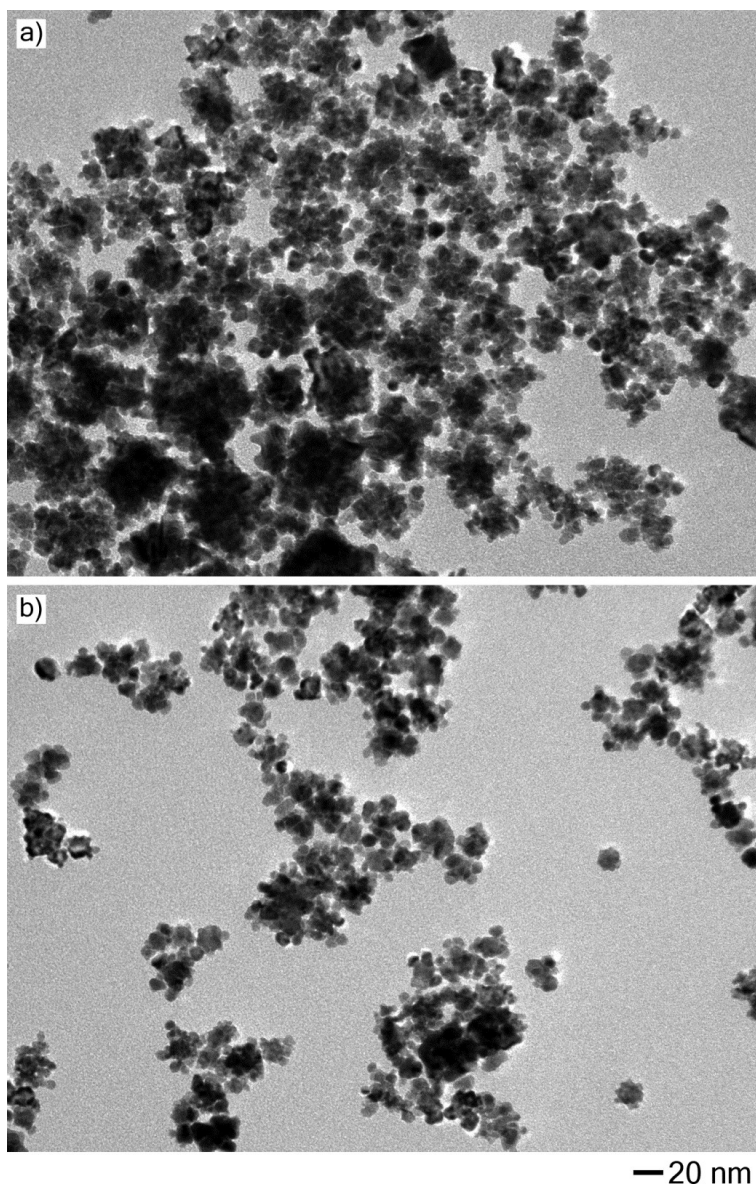


Figure S9. TEM images of Au@PdAu products obtained via the standard procedure, except that the volume of Au seed stock solution was varied to: a) 200 μ L and b) 500 μ L, respectively.

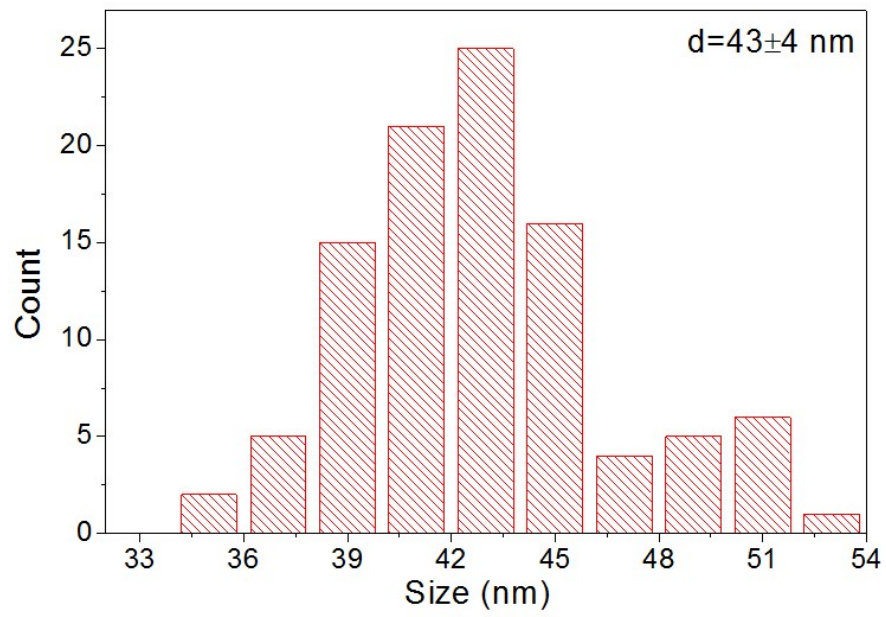


Figure S10. Histogram showing the size distribution of Au@PdAu core-shell nanocrystals in the form of segmented branches.

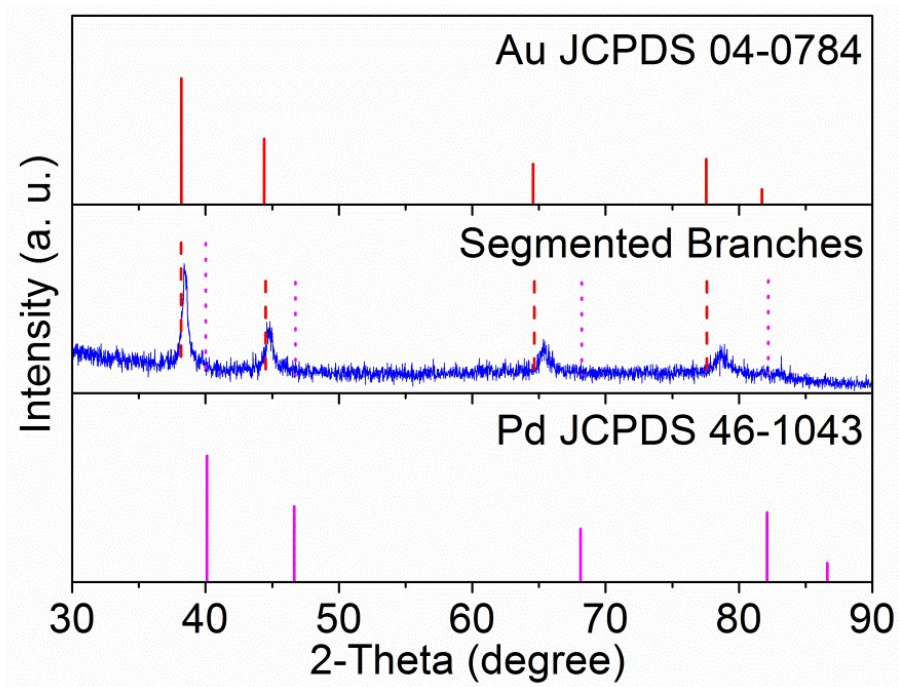


Figure S11. XRD pattern of Au@PdAu core-shell nanocrystals in the form of segmented branches.

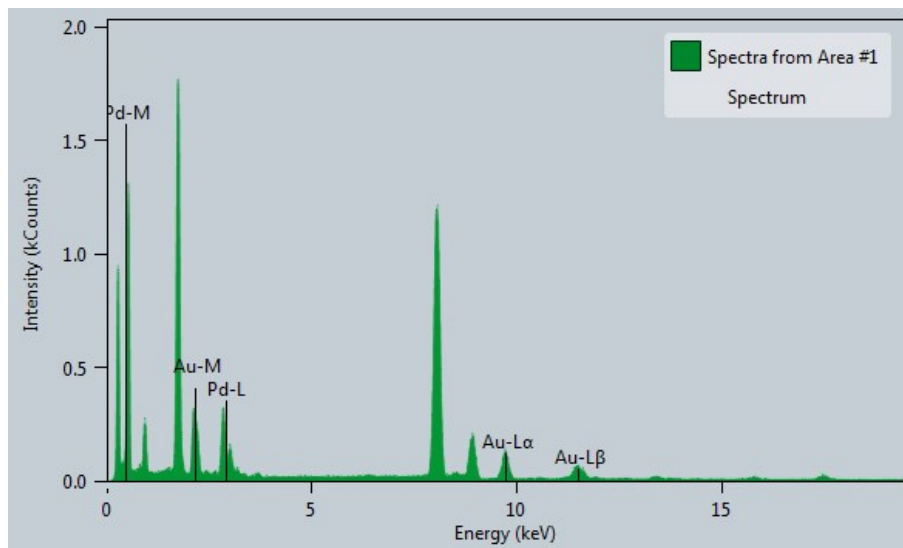


Figure S12. EDS spectrum of Au@PdAu core-shell nanocrystals in the form of segmented branches.

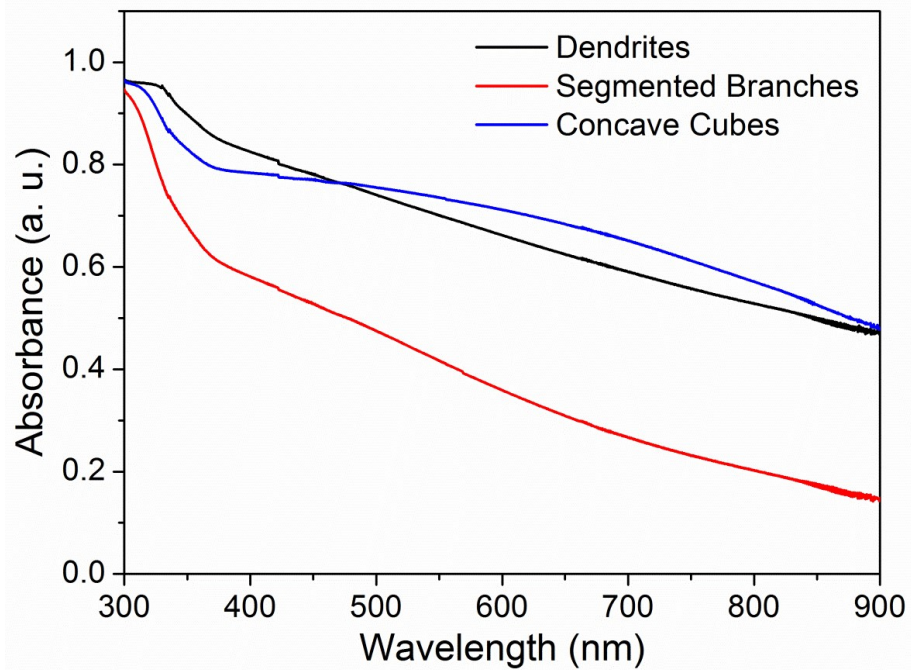


Figure S13. UV-vis extinction spectra of Au@PdAu nanocrystals with different morphologies.

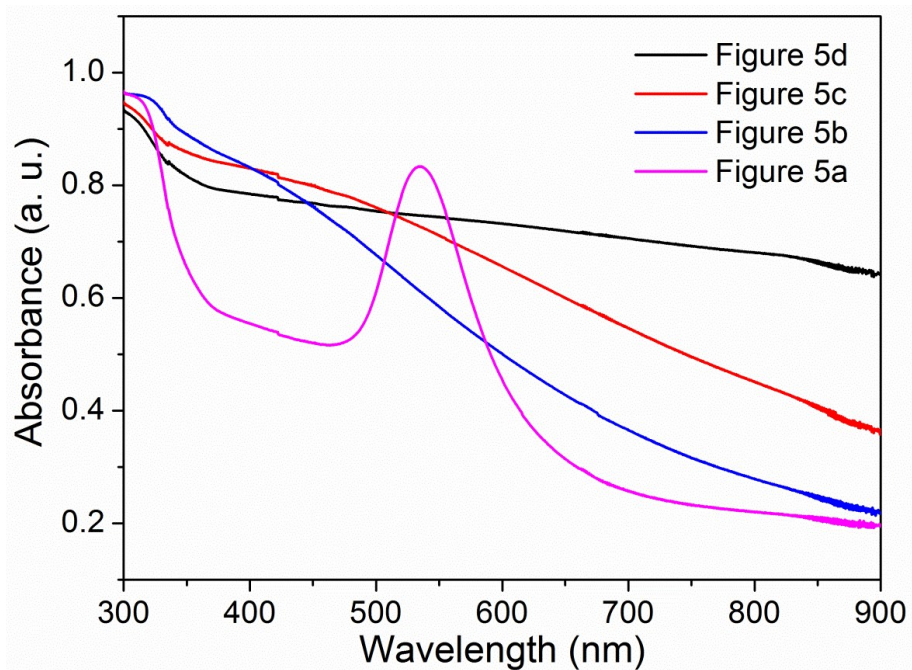


Figure S14. UV-vis extinction spectra of products as displayed in Figure 5.

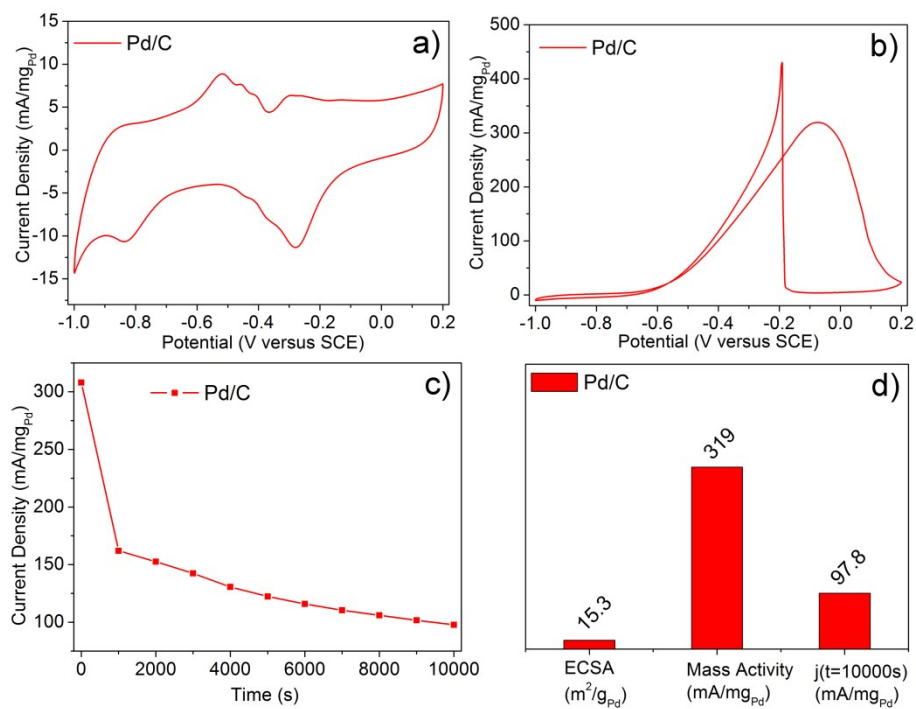


Figure S15. Electrochemical measurements of Pd/C catalysts for EOR: a) CV curve in 1 M KOH solution; b) CV curves in 1 M ethanol containing 1 M KOH; c) Chronoamperometric stability curves measured at -0.2 V versus SCE. d) Histograms showing the value of ECSA, mass activity, and $j(t=10000$ s).

Table S1. Synthetic parameters of products as displayed in current work.

Sample No.	CTAC (200 mM)	Seeds	Au/Pd Precursor			Precursor Injection Rate	AA (100 mM)	Temperature
			Concentration		Volume			
			H _{Au} Cl ₄	Na ₂ PdCl ₄				
Figure 1a	2 mL	20 μ L	0.5 mM	0.5 mM	2 mL	One-shot	0.2 mL	60 $^{\circ}$ C
Figure 1b	2 mL	20 μ L	0.5 mM	0.5 mM	2 mL	12 mL/h	0.2 mL	60 $^{\circ}$ C
Figure 1c	2 mL	20 μ L	0.5 mM	0.5 mM	2 mL	4 mL/h	0.2 mL	60 $^{\circ}$ C
Figure 1d	2 mL	20 μ L	0.5 mM	0.5 mM	2 mL	2 mL/h	0.2 mL	60 $^{\circ}$ C
Figure S1	2 mL	20 μ L	0.5 mM	0.5 mM	2 mL	1 mL/h	0.2 mL	60 $^{\circ}$ C
Figure 4b	2 mL	20 μ L	0.5 mM	0.5 mM	0.5 mL	2 mL/h	0.2 mL	60 $^{\circ}$ C
Figure 4c	2 mL	20 μ L	0.5 mM	0.5 mM	1 mL	2 mL/h	0.2 mL	60 $^{\circ}$ C
Figure 4d	2 mL	20 μ L	0.5 mM	0.5 mM	1.5 mL	2 mL/h	0.2 mL	60 $^{\circ}$ C
Figure 5a	2 mL	20 μ L	1 mM	0	2 mL	2 mL/h	0.2 mL	60 $^{\circ}$ C
Figure 5b	2 mL	20 μ L	0	1 mM	2 mL	2 mL/h	0.2 mL	60 $^{\circ}$ C
Figure 5c	2 mL	20 μ L	0.25 mM	0.75 mM	2 mL	2 mL/h	0.2 mL	60 $^{\circ}$ C
Figure 5d	2 mL	20 μ L	0.75 mM	0.25 mM	2 mL	2 mL/h	0.2 mL	60 $^{\circ}$ C
Figure 6	2 mL	20 μ L	0.5 mM	0.5 mM	2 mL	One-shot	0.2 mL	RT
Figure 7a	2 mL	20 μ L	0.5 mM	0.5 mM	2 mL	12 mL/h	0.2 mL	RT
Figure 7b	2 mL	20 μ L	0.5 mM	0.5 mM	2 mL	4 mL/h	0.2 mL	RT
Figure 7c	2 mL	20 μ L	0.5 mM	0.5 mM	2 mL	2 mL/h	0.2 mL	RT
Figure 7d	2 mL	20 μ L	0.5 mM	0.5 mM	2 mL	1 mL/h	0.2 mL	RT
Figure S9a	2 mL	200 μL	0.5 mM	0.5 mM	2 mL	2 mL/h	0.2 mL	60 $^{\circ}$ C
Figure S9b	2 mL	500 μL	0.5 mM	0.5 mM	2 mL	2 mL/h	0.2 mL	60 $^{\circ}$ C

Table S2. Summary of EOR catalytic performance for electrocatalysts in the present study.

Electrocatalyst	ECSA (m ² g _{Pd} ⁻¹)	Onset Potential (mV vs SCE)	Peak potential (mV vs SCE)	Mass Activity (mA mg _{Pd} ⁻¹)	<i>j</i> (t=10000s) (mA mg _{Pd} ⁻¹)
Au@PdAu CNCs/C	111	-971	-185	863	171
Au@PdAu SNBs/C	89.6	-957	-230	599	6.69
Au@PdAu NDs/C	81.2	-926	-165	663	411
Pd/C	15.3	-891	-75.0	319	97.8

References

1. Y. Zheng, X. Zhong, Z. Li and Y. Xia, *Part. Part. Syst. Character.*, 2014, **31**, 266-273.
2. Y. Zheng, Y. Ma, J. Zeng, X. Zhong, M. Jin, Z.-Y. Li and Y. Xia, *Chem. Asian J.*, 2013, **8**, 792-799.
3. W. Huang, X. Kang, C. Xu, J. Zhou, J. Deng, Y. Li and S. Cheng, *Adv Mater*, 2018, **30**, 1706962.